J|A|C|S
ARTICLES
Published on Web 02/27/2007

Atomic XAFS as a Tool To Probe the Reactivity of Metal Oxide Catalysts: Quantifying Metal Oxide Support Effects

Daphne E. Keller,[†] Sanna M. K. Airaksinen,[‡] A. Outi Krause,[‡]
Bert M. Weckhuysen,*[,†] and Diederik C. Koningsberger*[,†]

Contribution from the Inorganic Chemistry and Catalysis, Department of Chemistry, Utrecht University, P.O. Box 80083, 3508 TB Utrecht, The Netherlands, and Helsinki University of Technology, Laboratory of Industrial Chemistry, P.O. Box 6100, FIN-02015 HUT, Finland

Received September 20, 2006; E-mail: d.c.koningsberger@chem.uu.nl; b.m.weckhuysen@chem.uu.nl

Abstract: The potential of atomic XAFS (AXAFS) to directly probe the catalytic performances of a set of supported metal oxide catalysts has been explored for the first time. For this purpose, a series of 1 wt % supported vanadium oxide catalysts have been prepared differing in their oxidic support material (SiO_2, Al_2O_3, Nb_2O_5, and ZrO_2). Previous characterization results have shown that these catalysts contain the same molecular structure on all supports, i.e., a monomeric VO_4 species. It was found that the catalytic activity for the selective oxidation of methanol to formaldehyde and the oxidative dehydrogenation of propane to propene increases in the order $SiO_2 < Al_2O_3 < Nb_2O_5 < ZrO_2$. The opposite trend was observed for the dehydrogenation of propane to propene in the absence of oxygen. Interestingly, the intensity of the Fourier transform AXAFS peak decreases in the same order. This can be interpreted by an increase in the binding energy of the vanadium valence orbitals when the ionicity of the support (increasing electron charge on the support oxygen atoms) increases. Moreover, detailed EXAFS analysis shows a systematic decrease of the $V-O_b(-M_{support})$ and an increase of a the V−O(H) bond length, when going from SiO_2 to ZrO_2. This implies a more reactive OH group for ZrO_2, in line with the catalytic data. These results show that the electronic structure and consequently the catalytic behavior of the VO_4 cluster depend on the ionicity of the support oxide. These results demonstrate that AXAFS spectroscopy can be used to understand and predict the catalytic performances of supported metal oxide catalysts. Furthermore, it enables the user to gather quantitative insight in metal oxide support interactions.

1. Introduction

The catalytic performances of supported metal oxide catalysts are determined by many parameters, the most important being the metal oxide loading, pretreatment conditions, molecular structure, electronic structure, and support oxide type and composition.[1−5] Although many research groups have looked into the reactivity of supported metal oxide catalysts, it still remains unclear which of the above-mentioned parameters are truly responsible for the working of the catalyst material and how they are operative.

It has already been shown over the past decades that the catalytic activity in various oxidation reactions over supported metal oxide catalysts, e.g., chromium oxide, molybdenum oxide, tungsten oxide, and vanadium oxide based catalysts, changes with the support oxide composition.[1,3,6−8] For example, Cherian et al. have shown for supported chromium oxide catalysts that the turnover frequency (TOF) of the oxidative dehydrogenation of propane is a function of the support material and the TOF values increase 1 order of magnitude when the support is changed along the series: $Al_2O_3 \approx SiO_2-Al_2O_3 < SiO_2 \approx TiO_2$.[7] Methanol oxidation activity over supported molybdenum oxide catalysts exhibits a clear relationship with the nature of the support as well, and an increase of activity is observed according to the trend: $SiO_2 < NiO \approx Al_2O_3 < Cr_2O_3 < Nb_2O_5 < TiO_2 < MnO < ZrO_2$, which coincides with increasing Sanderson electronegativity values for the ions building up the support oxides.[9] In the case of the selective oxidation of methanol to formaldehyde over supported vanadium oxide catalysts, the TOF values are altered by 3 orders of magnitude simply by replacing the silica support oxide with a niobia support oxide.[1] Similar effects have been observed for the oxidative dehydrogenation of ethane and propane as well as for the selective oxidation of *n*-butane to maleic anhydride.[3,6,10] In order to explain these differences, Bañares and Wachs have

[†] Utrecht University.
[‡] Helsinki University of Technology.

(1) Deo, G.; Wachs, I. E. *J. Catal.* **1994**, *146*, 323−333.
(2) Olthof, B.; Khodakov, A.; Bell, A. T.; Iglesia, E. *J. Phys. Chem. B* **2000**, *104*, 1516−1528.
(3) Bañares, M. A. *Catal. Today* **1999**, *51*, 319−348.
(4) Burcham, L. J.; Wachs, I. E. *Catal. Today* **1999**, *49*, 467−484.
(5) Bañares, M. A.; Martínez-Huerta, M. V.; Gao, X.; Fierro, J. L. G.; Wachs, I. E. *Catal. Today* **2000**, *61*, 295−301.
(6) Khodakov, A.; Olthof, B.; Bell, A. T.; Iglesia, E. *J. Catal.* **1999**, *181*, 205−216.
(7) Cherian, M.; Someswara Rao, M.; Hirt, A. M.; Wachs, I. E.; Deo, G. *J. Catal.* **2002**, *211*, 482−495.
(8) Heracleous, E.; Machli, M.; Lemonidou, A. A.; Vasalos, I. A. *J. Mol. Catal. A: Chem.* **2005**, *232*, 29−39.
(9) Briand, L. E.; Farneth, W. E.; Wachs, I. E. *Catal. Today* **2000**, *62*, 219−229.
(10) Bañares, M. A.; Wachs, I. E. *J. Raman Spectrosc.* **2002**, *33*, 359−380.

10.1021/ja0667007 CCC: $37.00

discussed these differences in catalytic performances in terms of electronegativity differences between the cations of the support oxides comprising the catalyst materials.[10]

For supported noble metal particles the effect of the support oxide on the catalytic properties of metal nanoparticles has been determined via several spectroscopic techniques, and it has been shown that XPS, FT−IR on adsorbed CO, and atomic XAFS (AXAFS) spectroscopy appeared to be very helpful in this respect.[11−16] It has been shown with AXAFS that the influence of the support oxide acts through changes in the electron charge of the support oxygen atoms when the support composition is altered.[13] For example, in the case of supported Pt nanoparticles it was found that the ionization potential of Pt increases with increasing ionicity of the support oxide. Preferably, comparison of AXAFS from different catalyst materials is done on metal nanoparticles with similar sizes.

In order to apply AXAFS for studying metal oxide support interactions, metal oxide clusters with the same overall molecular structure are required. In general, the VO_4 monomeric species in dehydrated supported vanadium oxide catalysts has been envisaged as a distorted tetrahedral structure with one V═O bond and three V−O_b−$M_{support}$ bonds.[17−21] Although this classical VO_4 model is most widely accepted in literature, recent studies demonstrated, with results obtained from EXAFS at 77 K in combination with structural models, that for supported vanadium oxide species a single V−O_b−$M_{support}$ bond can be formed on alumina, silica, niobia, and zirconia supports.[22−24] The structure of the interface between the support oxide material and the VO_4 cluster has also been recently determined. As is depicted in Figure 1 the molecular structure of the supported vanadium oxide species consists of one V═O bond, 2 V−O(H) bonds, and one V−O_b−$M_{support}$ bond. The V−O(H) and V−$M_{support}$ distances depend on the support oxide material.[23−25] The consequence of this model is that if the same type of support oxide influence is present on the catalytic performance of vanadium as mentioned above for supported metal oxide catalysts, this must act via the V−O_b−$M_{support}$ bond.

In the present paper we have explored the possibilities of the AXAFS technique for the first time to study the influence of the support oxide on the local geometrical and electronic structure of a vanadium surface species. For this purpose, a series of low-loaded (1 wt %) supported (Al_2O_3, Nb_2O_5, SiO_2, and ZrO_2) vanadium oxide catalysts has been used, which were extensively characterized in our earlier papers.[23−25] The local structure around vanadium (i.e., 1 V═O, 1V−O_b−$M_{support}$, and two V−O(H) bonds)[23,24] was the same on all supports under investigation. However, the detailed EXAFS analysis carried out in this study will show that the bond length of the V−O_b-(−$M_{support}$) interaction decreases (with a simultaneous increase of the V−O(−H) bond) with increasing ionicity of the support (i.e., increasing electron charge on the support oxygen atoms). At the same time a systematic decrease of the vanadium FT AXAFS peak has been observed, which can be interpreted as an increase of the vanadium valence orbitals to a higher binding energy. This can be directly correlated with a change in the catalytic behavior of vanadium. The turnover number (TON) for propane dehydrogenation decreases, while those for the selective oxidation of methanol to formaldehyde and for the oxidative dehydrogenation of propane to propene increase with increasing ionicity of the support oxide. These results show that the increasing electron charge of the support oxygen atoms polarizes the V−O_b interaction with a simultaneous change in the reactivity of the catalytic V−O(−H) site. It is anticipated that the AXAFS technique will be able to explain the catalytic activity of other supported metal oxide catalysts in terms of differences in support ionicity as well and therefore can be regarded as a more generally applicable spectroscopic probe to investigate metal oxide support interactions.

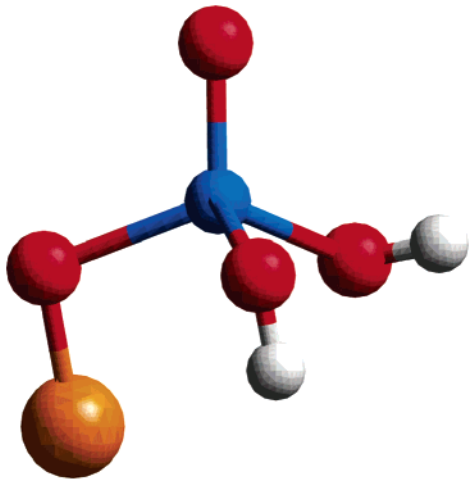

Figure 1. Schematic representation of the supported vanadium oxide species under study, which consists of a vanadium center consisting of one V═O, two V−O, and one V−O_b−$M_{support}$ bond.

2. Experimental Section

2.1. Catalysts Preparation. A series of low-loaded supported vanadium oxide catalysts was prepared making use of four different support oxides; i.e., Al_2O_3, Nb_2O_5, SiO_2, and ZrO_2. Both Al_2O_3 (S_{BET} = 165 m^2 g^{-1}, V_{pore} = 0.35 mL g^{-1}) and SiO_2 (S_{BET} = 600 m^2 g^{-1}, V_{pore} = 0.71 mL g^{-1}) were prepared via a sol−gel method described elsewhere.[23,24,26] Nb_2O_5 (HY-340, CBMM, S_{BET} = 188 m^2 g^{-1}, V_{pore} = 0.18 mL g^{-1}) and ZrO_2 (RC100, Gimex, S_{BET} = 100 m^2 g^{-1}, V_{pore} = 0.23 mL g^{-1}) were obtained from a commercial source. The 1 wt % V-based catalysts were prepared via incipient wetness impregnation of NH_4VO_3 (Merck, p.a.) with oxalic acid (Brocacef, 99.25%). The

(11) Mojet, B. L.; Miller, J. T.; Ramaker, D. E.; Koningsberger, D. C. *J. Catal.* **1999**, *186*, 373−386.
(12) Montes, C.; Davis, M. E.; Murray, B.; Narayana, M. *J. Phys. Chem.* **1990**, *94*, 6431−6435.
(13) Koningsberger, D. C.; de Graaf, J.; Mojet, B. L.; Ramaker, D. E.; Miller, J. T. *Appl. Catal. A: Gen.* **2000**, *191* (1,2), 205−220.
(14) Benvenutti, E. V.; Franken, L.; Moro, C. C. *Langmuir* **1999**, *15*, 8140−8146.
(15) van der Eerden, A. M. J.; Visser, T.; Nijhuis, T. A.; Ikeda, Y.; Lepage, M.; Koningsberger, D. C.; Weckhuysen, B. M. *J. Am. Chem. Soc.* **2005**, *127*, 3272−3273.
(16) Visser, T.; Nijhuis, T. A.; van der Eerden, A. M. J.; Jenken, K.; Ji, Y.; Bras, W.; Nikitenko, S.; Lepage, M.; Weckhuysen, B. M. *J. Phys. Chem. B* **2005**, *109*, 3822−3831.
(17) Wachs, I. E. *Catal. Today* **1996**, *27*, 437−455.
(18) Takenaka, S.; Tanaka, T.; Yamazaki, T.; Funabiki, T.; Yoshida, S. *J. Phys. Chem. B* **1997**, *101*, 9035−9040.
(19) Oyama, S. T.; Went, G. T.; Lewis, K. B.; Bell, A. T.; Somorjai, G. A. *J. Phys. Chem.* **1989**, *93*, 6786−6790.
(20) Eckert, H.; Wachs, I. E. *J. Phys. Chem.* **1989**, *93*, 6796−6805.
(21) Le Coustumer, L. R.; Taouk, B.; Le Meur, M.; Payen, E.; Guelton, M.; Grimblot, J. *J. Phys. Chem.* **1988**, *92*, 1230−1235.
(22) Keller, D. E., PhD thesis; *X-ray spectroscopy of supported vanadium oxide catalysts*; Utrecht Univeristy, 2006.
(23) Keller, D. E.; de Groot, F. M. F.; Koningsberger, D. C.; Weckhuysen, B. M. *J. Phys. Chem. B* **2005**, *109*, 10223−10233.
(24) Keller, D. E.; Koningsberger, D. C.; Weckhuysen, B. M. *J. Phys. Chem. B* **2006**, *110*, 14313−14325.
(25) Keller, D. E.; Visser, T.; Soulimani, F.; Koningsberger, D. C.; Weckhuysen, B. M. *Vibrational Spectrosc.* **2007**, *43*, 140−151.
(26) Weckhuysen, B. M.; de Ridder, L. M.; Schoonheydt, R. A. *J. Phys. Chem.* **1993**, *97*, 4756−4763.

Table 1. Catalyst Sample Codes, the Vanadium Oxide Loading Compared to the Monomeric and Polymeric Monolayer, and Data of the Support Oxide Material

sample name	sample	loading VO_x/nm^2	% monolayer[a] monomer	% monolayer[a] polymer	S_{BET} m^2/g	V_{pore} mL/g
1V−Si	1 wt % V_2O_5/SiO_2	0.118	5.13	1.57	594	0.71
1V−Al	1 wt % V_2O_5/Al_2O_3	0.430	18.7	5.73	165	0.35
1V−Nb	1 wt % V_2O_5/Nb_2O_5	0.399	17.3	5.32	188	0.18
1V−Zr	1 wt % V_2O_5/ZrO_2	0.743	32.3	9.91	100	0.23

[a] The values for the monomeric (2.3 VO_x/nm^2) and polymeric (7.5 VO_x/nm^2) monolayer coverages are taken from Khodakov et al.[6]

molar ratio of NH_4VO_3 and oxalic acid was 1:2. The catalysts were dried at room temperature for 1 night and at 393 K for 1 night at 393 K, and after that the catalysts were calcined at 773 K for 3 h. This resulted in catalyst materials with a vanadium oxide loading well below the monolayer coverage (∼7.5 VO_x/nm^2) for all support oxides.[6] All support oxides and prepared supported vanadium oxide catalysts are listed in Table 1, together with some physicochemical information as well as the catalyst codes that will be used throughout this paper.

2.2. Catalytic Experiments. The propane dehydrogenation activities were measured in a continuous flow microreactor system equipped with a Fourier Transform Infrared (FT−IR) gas analyzer for product analysis. The catalytic activity and TON for propane dehydrogenation were calculated from the amount of propane reacted. The values were corrected for any activity portrayed by the bare support material. The conversion and selectivity were measured in a continuous flow reaction system with a fixed bed quartz reactor. The catalyst was embedded between two layers of SiC grains. For each reaction 300 mg of catalyst or support (425−500 μm) were used. The samples were first heated to 393 K, kept there for about 5.5 h, then were heated to the reaction temperature which took about 5−6 h and kept there for 1−2 h before the experiments started. The catalysts were heated to the reaction temperature under 5% O_2/N_2 (the flow rate of air was 20 mL min^{-1}, and that of nitrogen, 60 mL min^{-1}). The propane dehydrogenation reaction was performed at 833 K at a propane WHSV of 1.72 h^{-1}. A 10%/90% reaction mixture of propane/N_2 was used for the reaction, with a flow rate of 43 mL min^{-1} in total. The reaction products were monitored with the FT−IR gas analyzer (Temet Instruments Ltd) with a Peltier-cooled mercury-cadmium-telluride detector. The spectra were collected over a wavenumber range of 4000−850 cm^{-1} with a resolution of 8 cm^{-1} at a scan rate of 10 scans s^{-1}. The analysis cuvette (9 cm^3) was kept at a constant temperature (180 °C) and pressure (103 kPa). Spectra were collected every other second during the first 2 min on stream, every 5 s during the next 2 min, and thereafter 2 spectra per min for the remainder of the measurement time. The FTIR analyzer allowed for a quantitative analysis of methane, ethane, propane, propene, CO, CO_2, and H_2O. The composition of the product stream was calculated using the Calcmet (Temet Instruments Ltd.) analysis program after calibration for the measured compounds. A detailed account of the method used for analyzing light hydrocarbons can be found elsewhere.[27]

2.3. EXAFS Spectroscopy. XAFS experiments were carried out at beamline E4 in Hasylab (Hamburg, Germany) using a Si (111) monochromator. The measurements were performed in fluorescence mode, using an ion chamber filled with 400 mbar N_2 to determine I_0. The detector was a 7-element solid state (SiLi) detector. The monochromator was detuned to 80% of the maximum intensity at the V K-edge (5465 eV) to minimize the presence of higher harmonics. The measurements were carried out in an in situ cell with Kapton windows. Details on the cell design can be found elsewhere.[28] Data were collected at 77 K after dehydration (623 K for 2 h in 2.5% O_2/He, 100 mL min^{-1}), and two to four scans were averaged.

Table 2. Activity (Ac) and Turnover Number (TON) for Propane Dehydrogenation (T = 833 K, $WHSV_{propane}$ = 1.72 h^{-1})[a]

sample name	propane dehydrogenation, 833 K: Ac	propane dehydrogenation, 833 K: TON
1V−Si	0.078	0.0074
1V−Al	0.028	0.0026
1V−Nb	<0[b]	<0[b]
1V−Zr	0.011	0.00096

[a] The conversion of propane varied between 0% and 4.5%. [b] For propane dehydrogenation over niobia-supported vanadium oxide catalysts, the support oxide activity exceeds the activity of the vanadium-containing catalyst.

The EXAFS data analysis was carried out using the XDAP code developed by Vaarkamp et al.[29] The background was subtracted employing cubic spline routines with a continuously adjustable smooth parameter.[30] In a separate paper this background subtraction procedure to separate the oscillatory part of the spectrum from the atomic background has been described in detail for different vanadium-containing reference samples.[31] Background subtraction led to the normalized oscillatory part of the XAFS data, for which all the contributions to the spectrum, including the AXAFS, were maximized.[30]

The EXAFS data-analysis program XDAP allows one to perform multiple-shell fitting in R-space by minimizing the residuals between both the absolute and the imaginary part of the Fourier transforms of the data and the fit. R-space fitting has important advantages compared to the usually applied fitting in k-space and is extensively discussed in a paper by Koningsberger et al.[30] The difference file technique was applied together with phase-corrected Fourier transforms to resolve the different contributions in the EXAFS data.[30] The details of the fit procedure on the vanadium EXAFS data have been described in previous papers by our research group.[23,24,31] In this study the FT AXAFS peak has been obtained by Fourier transforming the difference file, obtained by subtraction of the total fit from the raw data.

3. Results

3.1. Propane Dehydrogenation Activities. During the propane dehydrogenation reaction between <0 % (for 1V−Nb) and 4.5% of the propane is converted to reaction products by the vanadium oxide containing catalysts, depending on the support oxide material. Although during the dehydrogenation reaction propane is converted to propene, side products such as CO, CO_2, H_2O, ethane, methane, and coke are formed as well. When the formation of carbon-type (coke) species on the catalyst surface is disregarded, the selectivity to propene is between 90% and 100% for all catalysts under investigation.

The calculated activity and related TON of the propane dehydrogenation for the different supported vanadium oxide catalysts under study are listed in Table 2. It can be seen that the catalytic activity and TON are a function of the support oxide and follow the order Nb < Zr < Al < Si. It is important to stress that these values were determined at the end of a reaction cycle and that the activity and TON values were corrected for any activity portrayed by the bare support oxide material. Interestingly, the zirconia support used showed a very high activity compared to the vanadium-containing zirconia-based catalyst. Instead, the difference in activity between the

(27) Hakuli, A.; Kytökivi, A.; Lakomaa, E.-L.; Krause, A. I. O. *Anal. Chem.* **1995**, *67*, 1881−1886.
(28) Kampers, F. W. H.; Maas, T. M. J.; van Grondelle, J.; Brinkgreve, P.; Koningsberger, D. C. *Rev. Sci. Instrum.* **1989**, *60*, 2635−2638.
(29) Vaarkamp, M.; Linders, J. C.; Koningsberger, D. C. *Physica B* **1995**, *208/209*, 159.
(30) Koningsberger, D. C.; Mojet, B. L.; van Dorssen, G. E.; Ramaker, D. E. *Top. Catal.* **2000**, *10*, 143−155.
(31) Keller, D. E.; Weckhuysen, B. M.; Koningsberger, D. C. *Chem.−Eur. J.* **2007**, in press.

niobia support and vanadium-containing niobia-based catalyst is very small, although at the end of the cycle the activity of the bare support oxide was higher than that for the 1V−Nb sample, resulting in a catalytic activity below 0. The alumina support was also active for propane dehydrogenation; however, the activity of the vanadium-containing alumina-based catalyst was significantly larger than the bare support activity.

3.2. EXAFS Data Analysis. In previous papers we have determined the local structure of low-loaded (1 wt %) supported vanadium oxide catalysts with EXAFS measured at 77 K after dehydration treatment at 350 °C.[23,24] The structure of the interface with the SiO_2, Al_2O_3, Nb_2O_5, and ZrO_2 supports has been determined in detail as well. As is depicted in Figure 1 the vanadium center consists of one V═O bond, 2 V−O(H) bonds and one V−O_b−$M_{support}$ bond.[23−25] The V−O(H) and V−$M_{support}$ distances depend on the support material.[23,24] The details of the EXAFS characterization are summarized in the Supporting information.

Since the supported VO_4 cluster has only one bond to the surface of the SiO_2, Al_2O_3, Nb_2O_5, and ZrO_2 supports, it means that a support influence, if any, will act through this bond. So, one may expect a trend in V−O_b bond distance as a function of the electron charge of the support oxygen atom O_b. Consequently, the V═O and other two V−O(H) bond distances will change as well. In the earlier published EXAFS data analysis (see Table S1 in the Supporting Information) only two subshells in the first nearest neighbor shell were allowed in the EXAFS fits (V═$O_{(1)}$: CN = 1, representing the V═O bond; V−$O_{(2)}$: CN = 3, representing the two V−O(H) and one V−O_b−$M_{support}$ bonds). Here we have tried to carry out a more chemical realistic EXAFS data analysis by splitting the first nearest neighbor shell into three subshells: V═$O_{(1)}$, V−$O_{(2)}$: CN = 2, representing the two V−O(H) bonds; V−$O_{(3)}$: CN = 1 representing the V−O_b−$M_{support}$ bond. Since there is a strong overlap between the nearest and next nearest neighbor shells (arising from the support interface) it was necessary to include some support contributions in order to make the fit for V═$O_{(1)}$, V−$O_{(2)}$, and V−$O_{(3)}$ reliable. In the fit procedure the coordination number and distances of the support next nearest neighbor contributions were not allowed to vary, implying a known structure of the interface with the support. For V═$O_{(1)}$, a coordination number of 1 and $R = 1.58$ Å were used as fixed input parameters (in accordance with the Raman data and previous EXAFS analysis).[23,24,32] Furthermore, the coordination numbers for V−$O_{(2)}$ and V−$O_{(3)}$ were fixed to CN = 2 and CN = 1, respectively. The FT of the fits and the raw EXAFS data are shown in Figure 2a−d. The fits describe the data adequately in the applied range of values of *R*. However, it can be seen that at low values of *R* deviations exist due to the presence of the AXAFS oscillations, which are not included in the fit. The results of the fits are summarized in Table 2. It can be seen that the coordination distance of V−$O_{(2)}$ and V−$O_{(3)}$ are a function of the ionicity of the support oxide. An increase for V−$O_{(2)}$ and a decrease for V−$O_{(3)}$ are observed with increasing ionicity of the support oxide.

3.3. FT AXAFS Peak Intensity as a Function of the Ionicity of the Support Oxide. When the total fit is subtracted from the raw data, the residue remains. This residue contains the AXAFS contribution to the spectrum and the nonfitted higher shell contributions. Figure 3 shows the FT of the of the difference file in the AXAFS region ($0 < R < 1$ Å). It can be seen that the intensity of the FT AXAFS peak decreases systematically with increasing support ionicity. The centroid position of the FT AXAFS peak hardly changes; only a very small shift is observed to higher values of *R* (see Table 3).

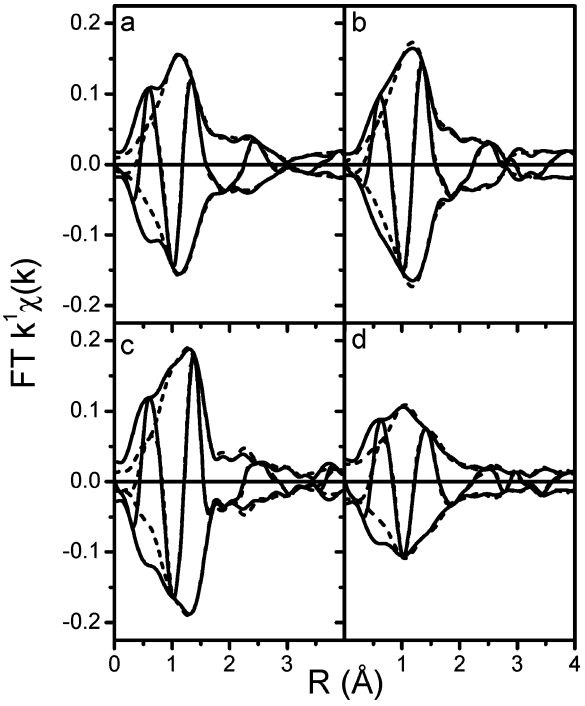

Figure 2. k^1 weighted Fourier transform ($\Delta k = 2.5-11$ Å^{-1}, ($\Delta R = 0.7-4.0$ Å) of the experimental $\chi(k)$ (—) and the final fit (- - -) for (a) 1V−Al; (b) 1V−Nb, (c) 1V−Si, and (d) 1V−Zr.

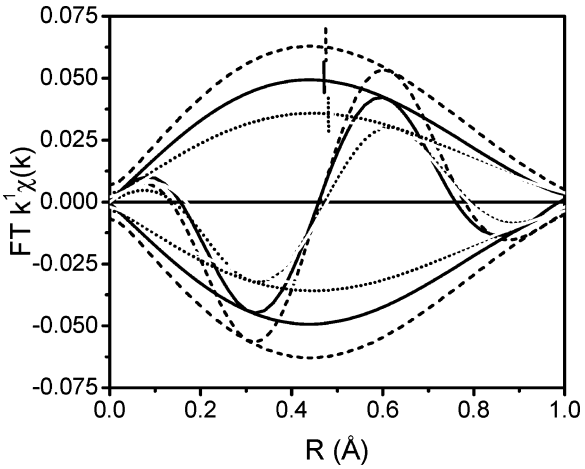

Figure 3. Residue (Raw − total fit), $\Delta k = 2.5-8$ Å^{-1}, in the AXAFS region ($0 < R < 1$ Å) with the centroid position of the AXAFS peak for 1V−Si (- - -), 1V−Al (black solid line), 1V−Nb (···) and 1V−Zr (gray solid line).

4. Discussion

4.1. Influence of the Ionicity of the Support Oxide on the Molecular Structure of Supported Vanadium Oxide Species. All catalysts discussed in this paper were thoroughly investigated with various spectroscopic techniques after dehydration treatment in previous papers.[23−25] From the Raman, UV−vis, and ESR data on low-loaded (1 wt %) supported vanadium oxide catalysts it could be concluded that the vanadium oxide was

(32) Hardcastle, F. D.; Wachs, I. E. *J. Phys. Chem.* **1991**, *95*, 5031−5041.

Table 3. Structural Parameters from R-Space Fits of the Experimental EXAFS for Samples 1V−Si, 1V−Al, 1V−Nb, and 1V−Zr with the Second Shell Split into Two Shells: V−O_b and V−O(H)[a]

fit	scattering pair	CN[b]	R^b (Å)	$\Delta\sigma^{2\,b}$	$\Delta E_0{}^b$	$N_{free}{}^b$	$N_{fit}{}^b$	variances % imaginary part	variances % absolute part
1V−Si	V═$O_{(1)}$	1*	1.58*	−0.000 03	7.57	11.7	10	4.2	2.7
	V−$OH_{(2)}$	2*	1.69	−0.001 86	7.24				
	V−$O_{b(3)}$	1*	1.80	−0.001 50	1.60				
	V---$Si_{(4)}$	1*	2.61*	0.012 00	5.06				
1V−Al	V═$O_{(1)}$	1*	1.58*	−0.003 13	6.87	15.5	12	1.1	0.97
	V−$OH_{(2)}$	2*	1.715	0.003 24	10.63				
	V−$O_{b(3)}$	1*	1.73	0.004 00	−1.08				
	V---$O_{(4)}$	1*	2.29*	0.015 00	−1.22				
	V---$Al_{(5)}$	1*	3.10*	0.011 86	6.12				
1V−Nb	V═$O_{(1)}$	1*	1.58*	−0.0250	4.58	13.4	12	1.4	0.84
	V−$OH_{(2)}$	2*	1.72	0.002 00	5.00				
	V−$O_{b(3)}$	1*	1.68	0.000 93	12.87				
	V---$O_{(4)}$	1*	2.43*	0.002 17	2.67				
	V---$Nb_{(5)}$	1*	2.64*	0.006	15.00				
1V−Zr	V═$O_{(1)}$	1*	1.58*	−0.001 20	8.95	11.7	12	1.3	1.0
	V−$OH_{(2)}$	2*	1.81	0.006 26	4.85				
	V−$O_{b(3)}$	1*	1.675	0.005 00	9.32				
	V---$O_{(4)}$	1*	2.38*	0.015 00	−6.95				
	V---$O_{(5)}$	1*	2.64*	0.008 42	−4.79				

[a] Δk = 2.5 −11 for all samples; ΔR = 0.7−2.5 for sample 1V−Si, ΔR = 0.7−3.2 Å for 1V−Al, ΔR = 0.7−2.8 for 1V−Nb, and ΔR = 0.7−2.5 for 1V-Zr. [b] CN = coordination number, R = distance, $\Delta\sigma^2$ = Debye−Waller factor, i.e., disorder, E_0 = inner potential. Parameters marked with * are fixed during the fit. N_{free} is the maximum number of free parameters according to the Nyquist theorem, and N_{fit} is the number of parameters used in the fit.

Table 4. AXAFS Intensity and Centroid Position for the Different Catalyst Materials under Study

sample name	I_{AXAFS}	$R_{centroid}$, Å
1V−Si	0.060	0.4756
1V−Al	0.052	0.4698
1V−Nb	0.038	0.4811
1V−Zr	0.032	0.4891

present as V^{5+} in a fourfold coordination (Table 4). A detailed EXAFS analysis showed that the vanadium oxide catalysts measured at 77 K after dehydration treatment at 350 °C has only one bond to the surface on alumina, silica, niobia, and zirconia.[23,24] Since it is not possible to discriminate with EXAFS between different types of oxygen nearest neighbor groups (O, O(H), or O═O), the nature of the remaining V−O bonds in our newly proposed model with only one V−O_b−$M_{support}$ bond has been determined with a careful Raman and IR study.[25] In summary, our earlier studies concluded the presence of a distorted tetrahedral monomeric V^{5+} species with one V═O, one V−O_b−$M_{support}$, and two V−O(H) bonds under the measurement conditions applied.

The extended EXAFS data analysis of the first nearest neighbor shell as carried out in this study was inspired by the earlier observed changes in the $\Delta\sigma^2$ of the nearest neighbor shell as a function of the support ionicity (see Appendix). The change in V═O bond distance can be estimated from the Raman frequency of this bond.[32] Although the changes in frequency with the support oxide material are apparent (Table 4), the corresponding change in bond distance is smaller than 0.01 Å. Such small deviations in bond distance cannot be determined reliably with EXAFS. However, the V−O_b and V−O(H) distances are expected to exhibit larger changes in bond distances, and these may be determined with EXAFS. Therefore the original V−O_2 coordination has been split into the two subshells V−$O_{(2)}$: CN = 2, representing the two V−O(H) bonds and V−$O_{(3)}$: CN = 1 representing the V−O_b−$M_{support}$ bond. It can be seen in Table 3 that the coordination distance of V−$O_{(2)}$ and V−$O_{(3)}$ are indeed a function of the ionicity of the support oxide. The average distances of the split shells correspond to the values found in our original EXAFS data analysis. An increase for V−$O_{(2)}$ and a decrease for V−$O_{(3)}$ is observed with increasing ionicity of the support oxide in the order SiO_2 < Al_2O_3 < Nb_2O_5 < ZrO_2. From this result it can be concluded that the influence of the support oxide on the electronic and catalytic properties of the vanadium center act through the single V−O_b−$M_{support}$ bond.

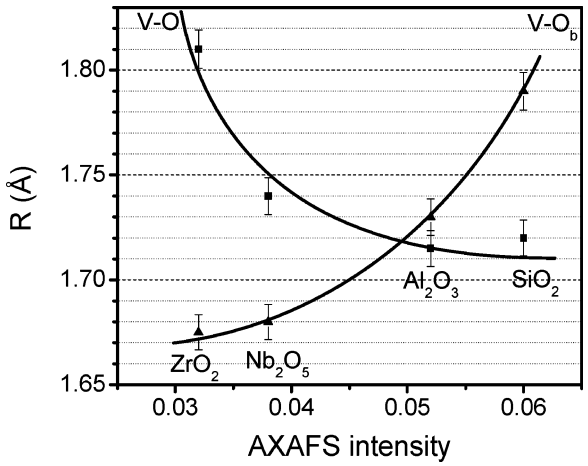

Figure 4. V−O_b and V−O bond distances as a function of the AXAFS intensity.

4.2. Influence of the Support Oxide on the Electronic Structure of Supported Vanadium Oxide Species. It is now instructive to plot the changes in the V−O(H) and the V−O_b−M bonds as a function of the AXAFS intensity. It can be seen in Figure 4 that a decreasing AXAFS intensity results in a decrease of the V−O_b distance and an increase of the V−O(H) bond length in the supported vanadium oxide species. From this

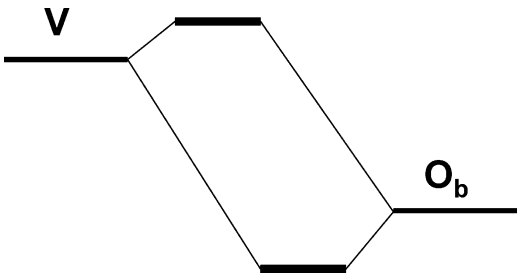

Figure 5. Schematic MO diagram of the V−O_b interaction.

observation it can be concluded that the decrease in AXAFS intensity is related to an increase in support oxide ionicity.

In the case of supported metal nanoparticles similar particle sizes are required to allow a comparison of the AXAFS intensity and centroid position as a function of the ionicity of the support oxide. Since the overall local structure of the supported vanadium oxide species is identical on all support oxides our systems are suitable for a comparison of their AXAFS parameters.[23,24] In other words, Figure 4 suggests strongly that the variations in the AXAFS parameters are related to a change in both the electronic and geometric structure of vanadium induced by a change in the ionicity of the support oxide.

4.2.1. Intuitive MO Diagram. Since the results suggest that the effect of the ionicity of the support (i.e., the electron charge of the support oxygen atoms) acts via the V−O_b−$M_{support}$ bond, it is instructive to make use of a schematic MO diagram as shown in Figure 5. For a support with a high ionicity (like ZrO_2) the electron charge of the oxygen anions is large ($O_b^{\delta-}$), implying that the position of the O_b binding orbital moves up to lower binding, making the V−O_b bond more covalent (stronger), and this results in a shorter bond length, as experimentally observed (see Figure 4). This means also that less electron density is shared in the V−OH bonds, which result in a longer V−O distance (see also Figure 4). This intuitive MO diagram explaining the decrease in the V−O_b bond length with increasing support ionicity is based upon charge transfer and possible polarization (see below) of the V−O_b bond. Figure 4 makes clear that a justification of the intuitive MO diagram as presented in Figure 5 must be found in an explanation of the decrease in the AXAFS intensity (with no observable change in centroid position) with increasing electron charge of the support oxygen atoms. The connection between changes in position of atomic orbitals (thereby influencing the MO scheme) and changes in AXAFS intensity has to be found in alterations of the interatomic potential around the X-ray absorbing atom V as discussed below.

4.2.2. AXAFS Intensity and Centroid Position. The effects determining the AXAFS can be described using the Muffin-Tin approximation to approximate the embedded atom potential.[33−35] Within the well-known Muffin-Tin approximation, the potential is flat and zero in the interstitial region ($R > R_{mt}$) and otherwise equal to the sum of overlapping, spherically symmetric potentials ($R < R_{mt}$). The average potential of all atoms at R_{mt} is V_{int}, which determines the zero of energy or the effective bottom of the conduction band in metals or the filled valence orbitals in metal oxides. The AXAFS is now determined by the difference (ΔV) between the embedded atom potential (V_{emb}) and the truncated free atom potential (V_{TFA}),[36] which lead to the following mathematical description: $|FT(ke^{-2i\delta}\chi_{AX})| \approx \Delta V \bullet \Gamma$. Since the potential of the embedded absorber atom is influenced by its direct surroundings, i.e., neighboring atoms, four parameters can influence the electronic properties of the absorber atom.[11,13,31,34,35,37−39]

(1) The average distance to the surrounding atoms: this results in changes in interaction between the absorber atom and the neighbors and thus alters the shape of the coulomb tail or rollover.

(2) The bond inductive effect, determined by the average of electronic properties of the neighboring atoms (e.g., electronegativity). Variations in the electronic properties of the neighboring atoms lead to variations in V_{int}.

(3) The coulomb effect, i.e., changes in the electron density of the neighboring oxygen atoms, alters the coulomb tail or rollover of the neighboring atom potential and thus the potential of the absorber atom. V_{int} changes as well, since the overall potential of the surrounding oxygen atoms is altered.

(4) Charge transfer to the absorber atom. The charge transfer induces variations in the absorber atom potential, hereby causing changes in the rollover and some variation in the V_{int}.

AXAFS has been used to study adsorbates on single-crystal surfaces[40] and on Pt electrodes[37,41] and metal support interactions in supported Pt particles.[11,13,15,38,42] The effect of the four parameters listed above on the AXAFS intensity and centroid position of different vanadium-containing reference samples has been extensively discussed in a separate paper.[31] In this work the FT AXAFS peak of vanadium has been shown to decrease with increasing ionicity of the supporting oxide (Table 3 and Figure 4). The centroid position shows only a very small shift to higher values of R when the support is changed from silica to zirconia. The trends observed in AXAFS intensity, and $R_{centroid}$ can now be discussed with regard to a change in the potential field around vanadium (middle and lower part of Figure 6). Variations in the electron charge (δ^-/δ^+) of the support oxygen lead to a polarization of the V−O_b bond ($V^{\delta+}$−$O_b^{\delta-}$/$V^{\delta-}$−$O_b^{\delta+}$) (upper part of Figure 6). An increased electron charge on the oxygen ($O_b^{\delta-}$) causes an upward shift in the oxygen potential well to lower binding energies, as in the case for ZrO_2 (left side of middle part of Figure 6). This decreases the influence of oxygen on the vanadium (less rollover) and thus the difference (ΔV) in the embedded potential and the truncated free atom potential, thereby decreasing the intensity of the FT AXAFS peak. At the same time, the net electron charge on vanadium

(33) Rehr, J. J.; Booth, C. H.; Bridges, F.; Zabinsky, S. I. *Phys. Rev. B* **1994**, *49*, 12347−123350.
(34) Ramaker, D. E.; Qian, X.; O'Grady, W. E. *Chem. Phys. Lett.* **1999**, *299*, 199.
(35) Ramaker, D. E.; Mojet, B. L.; Koningsberger, D. C.; O' Grady, W. E. *J. Phys. Condens. Matter* **1998**, *10*, 8753−8770.

(36) V_{TFA} is the free atom potential truncated by V_{cut}. V_{cut} is defined as $V_{cut} = 2xV_{int} + |E_{fermi}|$ and determines the minimum binding energy of the electrons that will be effective in scattering photoelectrons. So only the deeper localised valence band electrons give rise to AXAFS scattering (see ref 35).

(37) O' Grady, W. E.; Qian, X.; Ramaker, D. E. *J. Phys. Chem. B* **1997**, *101*, 5624−5626.
(38) Koningsberger, D. C.; de Graaf, J.; van Veen, J. A. R.; Ramaker, D. E. *J. Catal.* **2001**, *203*, 7−17.
(39) Tromp, M.; van Bokhoven, J. A.; Slagt, M. Q.; van Koten, G.; Ramaker, D. E.; Koningsberger, D. C. *J. Am. Chem. Soc.* **2004**, *126*, 4090−4091.
(40) Wende, H.; Srivastava, P.; Chauvistre, R.; May, F.; Barberschke, K.; Arvanitis, D.; Rehr, J. J. *J. Phys. Condens. Matter* **1997**, *9*, L427−L433.
(41) Roth, C.; Benker, N.; Buhrmester, T.; Mazurek, M.; Loster, M.; Fuess, H.; Koningsberger, D. C.; Ramaker, D. E. *J. Am. Chem. Soc.* **2005**, *127*, 14607−14615.
(42) Koningsberger, D. C.; Oudenhuijzen, M. K.; van Bokhoven, J. A.; Ramaker, D. E. *J. Catal.* **2003**, *216*, 178−191.

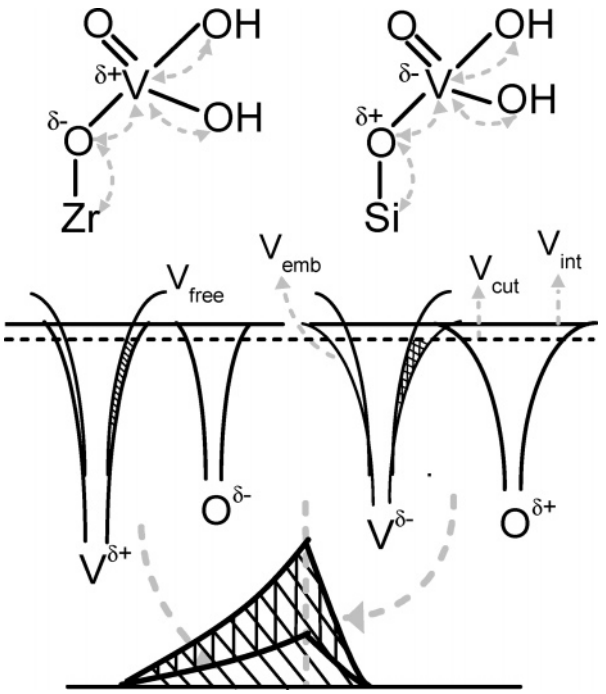

Figure 6. (Upper part) Polarization and charge transfer (indicated by arrows) (as described above with the intuitive MO picture in Figure 5) of the VO_4 cluster due to a change in electron charge of the support oxygen atoms ($O^{\delta-}$: high ionicity, ZrO_2 or $O^{\delta+}$: low ionicity, SiO_2). (Middle part) Schematic representation of the influence of the electron charge of the support oxygen atoms on the shape and position of the vanadium and oxygen potential wells (V_{free} = free atom potential, V_{emb} = embedded atom potential; for V_{int} and V_{cut}, see text above and ref 35). (Lower part) Schematic representation of the AXAFS FT peak. The intensity of this AXAFS peak is determined by the difference between V_{free} and V_{emb}, truncated by V_{cut} (see shaded area in the middle part of Figure 6).

decreases in a way as explained above using the intuitive MO picture (more V electron density is shared in the V−O_b bond). This leads to a smaller value of V_{cut} (V_{cut} moves to lower binding energy). The polarization causes the potential well of vanadium to shift down to higher binding energies ($V^{\delta+}$), i.e., an increase in ionization potential of vanadium, resulting in a slight increase in the rollover. The combination of these two effects hardly changes the position in energy of V_{cut} as is illustrated by the same position of the dotted line in Figure 6. This causes only small changes in the resulting centroid position of the FT AXAFS peak as a function of the supporting oxide, as has been observed. Furthermore, the resulting V−O interaction leads to a diminished rollover. The observed small change in centroid position of the FT AXAFS peak implies an almost constant position in energy of V_{cut}. As discussed above this can only be explained by a shift to higher binding energies of the vanadium valence orbitals with increasing ionicity of the supporting oxide. This shows that the observed changes in the FT XAFS peak are caused by a change in the electronic structure of vanadium induced by a change in ionicity of the supporting oxide.

It is has to be noted that in our previous studies[11,13,38,42] of metal support effects in supported Pt metal particles the influence of the electron charge of the support oxygen anions acts via a polarization of the Pt metal particles. Our previous study[39] of the influence of the electronegativity of the organometallic ligands in Pt pincer complexes on the AXAFS shows

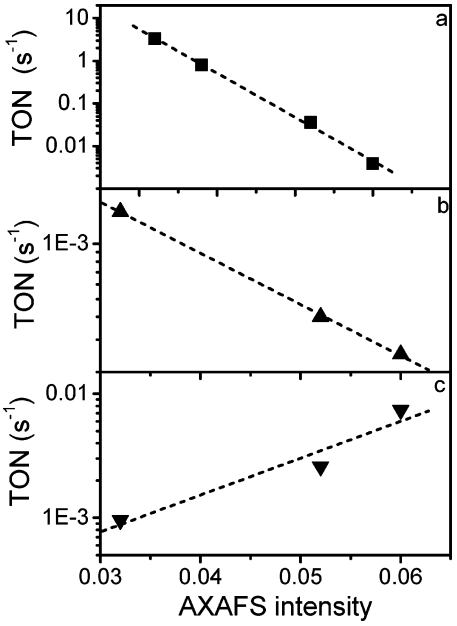

Figure 7. Correlation between the AXAFS intensity and the catalytic activity for (a) the selective oxidation of methanol to formaldehyde,[1] (b) the oxidative dehydrogenation of propane to propene, and (c) the dehydrogenation of propane to propene.

that charge transfer changes the electronic structure of Pt. In both cases a clear shift in position of the centroid of the AXAFS FT peak is observed. Since in this study no noticeable change is observed in the centroid position of the AXAFS FT peak, it must be concluded from the above discussion that the influence of the ionicity of the support on the geometrical and electronic properties of the VO_4 oxide cluster consists of both polarization and charge transfer.

4.3. Correlation between the AXAFS Probe and Catalytic Activity. First of all, it is important to keep in mind that the molecular structure was not determined under reaction conditions and the structure of the active species may be somewhat different from the one determined here. However, the AXAFS technique indicates a change of the electronic structure of vanadium as a function of the support oxide. It has been shown in this study that this change in electronic structure, acting via the V−O−$M_{support}$ bond, influences the reactivity of the V−O(H) oxygen groups surrounding the vanadium. The support oxide can affect the catalytic properties of the vanadium oxide, as has been demonstrated in the literature in the past.[1,3,6,10] The methanol oxidation data of the group of Wachs,[1] the literature data for oxidative dehydrogenation of propane by Khodakov,[6] and our propane dehydrogenation data have been used to determine a relationship between the AXAFS intensity and the catalytic activity for oxidation/reduction reactions.

The correlation between the TON and the AXAFS intensity is shown in Figure 7. A clear trend is observed for the methanol oxidation, oxidative dehydrogenation, and propane dehydrogenation.

The activity for methanol oxidation and oxidative dehydrogenation increases, while the activity for propane dehydrogenation decreases with increasing ionicity of the support oxide (Si < Al < Nb < Zr). This demonstrates that the AXAFS intensity of the catalysts determined at 77 K (after dehydration treatment) can be related to the catalytic activity of the supported vanadium oxide species.

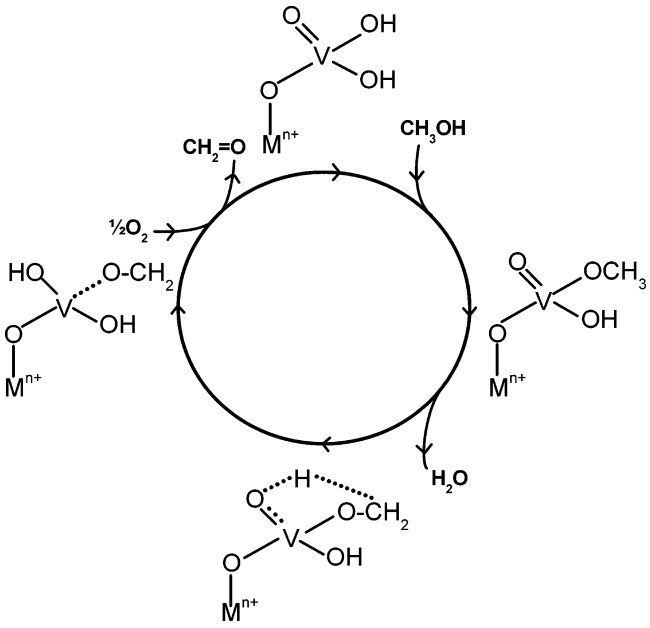

Figure 8. Schematic representation of a tentative reaction cycle for the selective oxidation of methanol to formaldehyde over supported vanadium oxide catalysts, represented by the Si−O−V(OH)$_2$O surface species.

Several research groups have looked into possible methanol oxidation mechanisms on bulk and supported vanadium oxides.[1,43−48] Recently, Döbler et al. studied methanol oxidation over a silica-supported vanadium oxide model ((Si−O)$_3$V═O) with density functional theory.[48] They suggest that the dissociative adsorption of methanol on one of the V−O−M$_{support}$ bonds is the first reaction step, yielding a methoxy group on the vanadium oxide cluster. Subsequently, hydrogen transfer takes place from the CH_3 group to the V═O group. They suggest that the V═O group is involved in the methanol oxidation. Furthermore, Döbler et al. propose that the differences in catalytic activity as a function of the support oxides are related to the first reaction step: i.e., the dissociative adsorption step of methanol. Our model is different in molecular structure from the classical model ((Si−O)$_3$V═O) and does not require the breaking of a V−O−M$_{support}$ to facilitate the adsorption of methanol on the vanadium oxide cluster. The adsorption of methanol may take place on the V−OH groups of the cluster under formation of a methoxy group, as has been suggested in the past by Busca.[46] We have shown that the V−OH distances depend on the support oxide material (Figure 4 and Table 2), which explains the differences in catalytic activity as a function of the support oxide in a similar way as that suggested by Döbler et al. Moreover, by accepting the transition state proposed in Döbler's paper, a tentative oxidation mechanism can be drawn as is shown in Figure 8. The oxygen atom in the V═O bond is exchanged, explaining the $^{16}O/^{18}O$ isotopic labeling experiments reported in literature.[34]

Finally, our findings allow us to explain the differences in reactivity intuitively in terms of V−(OH) and (V−)O−H bond distances (see Figure 4). The support cation changes the electronic properties of the O (δ^+/δ^-) in the V−O$_b$−M$_{support}$ bond. The V−O$_b$ bond length is a function of the support oxide and thus of the O$_b$ electronic properties (O$^{\delta-}$: short V−O$_b$ bond (on ZrO_2) and O$^{\delta+}$: long V−O$_b$ bond (on SiO_2)). The simple concept of conservation of bond order allows us to deduct that the V−(OH) and the (V−)O−H bond lengths will systematically change with the support oxide material as well, as we have shown for the V−(OH) distance (ZrO_2: long V−(OH), short (V−)O−H; SiO_2: short V−(OH), long (V−)O−H). In the case of methanol oxidation and propane oxidative dehydrogenation, H_2O formation may suggest that the V−(OH) group plays an important role in the catalytic reaction. Indeed, the vanadium oxide species with the longest V−(OH) bond exhibits the highest oxidation activity (1V − Zr). In contrast, the dehydrogenation of propane results in the formation of H_2 and shows an opposite trend in TON (Figure 6), suggesting that not the OH groups as a whole but the hydrogen atom from the V−OH group plays a role in the catalytic reaction. Although the exact mechanism of propane dehydrogenation has not been investigated in this study, a striking relation between the deducted trend in (V−)O−H bond length and catalytic activity has been observed (SiO_2: long O−H bond, high TON; ZrO_2: short O−H, low TON). Even though a clear relation could be established between the AXAFS intensity and the TON for a different reaction, one should keep in mind that the molecular structure determined for the supported vanadium oxide species (after dehydration, at 77 K) may differ from the structure of the catalytically active species (under reaction conditions).

This AXAFS study suggests that a change in the ionicity of the support changes the bonding of the reacting adsorbate (i.e., methanol) on the catalytic active site of the VO_4 species. It is not the first time that a correlation has been found between AXAFS intensity and catalytic reactivity. In our earlier study on metal support effects on supported Pt particles[42] the support alters the chemisorption of H and does not change directly the binding of the reacting alkane. It therefore has to be noted that the mechanism of the influence of the support on the activity of the catalytic active species can be very different.

5. Conclusions

On all support oxides under investigation, SiO_2, Al_2O_3, Nb_2O_5, and ZrO_2, the overall molecular structure of the surface vanadium oxide species is the same; i.e., a fourfold oxygen coordination. The V−O$_b$ distance increases from 1.675 Å to 1.79 Å when the support oxide is changed from ZrO_2 to SiO_2, while the V−O(H) distances decrease from 1.81 Å to 1.72 Å. The influence of the ionicity of the support on the bond distances correlates with the differences observed in catalytic performances of these supported vanadium oxide catalysts.

The electronic structure of the vanadium oxide species has been studied with AXAFS. The variations in the intensity and the observed changes in centroid position of the FT AXAFS peak as a function of the support ionicity can be explained by assuming both a coulomb effect, i.e., variation in charge on the surrounding support oxygen atoms, and variation of the binding energy of the valence orbitals of vanadium. A clear trend was observed between the intensity of the FT AXAFS peak and the

(43) Weckhuysen, B. M.; Keller, D. E. *Catal. Today* **2003**, *78*, 25−46.
(44) Burcham, L. J.; Braind, L. E.; Wachs, I. E. *Langmuir* **2001**, *17*, 6164−6174.
(45) Burcham, L. J.; Deo, G.; Gao, X.; Wachs, I. E. *Top. Catal.* **2000**, *11/12*, 85−100.
(46) Busca, G. *J. Mol. Catal.* **1989**, *50*, 241−249.
(47) Boulet, P.; Baiker, A.; Chermette, H.; Gilardoni, F.; Volta, J. C.; Weber, J. *J. Phys. Chem. B* **2002**, *106*, 9659−9667.
(48) Döbler, J.; Pritzsche, M.; Sauer, J. *J. Am. Chem. Soc.* **2005**, *127*, 10861−10868.

catalytic activity for the selective oxidation of methanol to formaldehyde, the oxidative dehydrogenation of propane, and the dehydrogenation of propane: the lowest intensity is correlated with the highest activity in oxidation reactions, and the highest intensity, with the highest activity for dehydrogenation reactions. These trends suggest that the AXAFS intensity can be used to understand and predict the catalytic performances of supported metal oxide catalysts in general.

Acknowledgment. The authors acknowledge the helpful discussions with Prof. Ramaker, George Washington University. The work at HASYLAB was supported by the IHP Contract HPRI-CI-2001-00140 of the European Commission. The authors acknowledge financial support from the EU-COST D15 program. B.M.W. acknowledges financial support from NRSCC, NWO/CW-van der Leeuw, NWO/CW-VICI, and CONCORDE.

Supporting Information Available: In the Supporting Information a table is available containing EXAFS fit results for all dehydrated catalysts. This material is available free of charge via the Internet at http://pubs.acs.org.

JA0667007